THE JOURNAL OF PHYSICAL CHEMISTRY B

Article

pubs.acs.org/JPCB

Reaction Mechanism of Monoamine Oxidase from QM/MM Calculations

Enrique Abad, Roland K. Zenn, and Johannes Kästner*

Computational Biochemistry Group, Institute of Theoretical Chemistry, University of Stuttgart, Pfaffenwaldring 55, 70569 Stuttgart, Germany

Supporting Information

ABSTRACT: The flavoenzyme monoamine oxidase (MAO) is essential for the enzymatic decomposition of neurotransmitters. While it is commonly accepted that the rate limiting step of the reaction is the stereoselective abstraction of a hydrogen from the substrate, the precise mechanism is unknown. We modeled the reaction of human MAO-B with benzylamine by means of QM/MM calculations based on density functional theory. Oxidation of the unprotonated substrate was found to proceed with rates in good agreement with experimental values, while the protonated substrate does not react at room temperature. Our results support a concerted asynchronous polar nucleophilic mechanism. The lone pair of the amine-nitrogen interacts with a carbon atom of the flavin cofactor. During the reaction, this lone pair, as well as a proton, are transferred to the cofactor. Analysis of the electronic structure during the reaction rules out a radical mechanism.

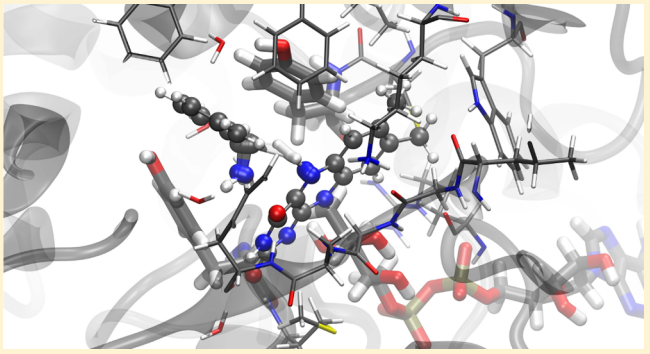

INTRODUCTION

The oxidative deamination of a large range of neurotransmitters (such as dopamine and serotonin) is carried out by monoamine oxidase (MAO, EC 1.4.3.4). MAO is a mitochondrial outer membrane flavoenzyme that is present in two different forms: MAO-A and MAO-B, with a sequence identity of about 70%.[1] These enzymes have been widely studied in the past because of the antidepressant properties of MAO inhibitors.[2] In the past few years, it has been found that the amount of MAO-B increases with age in humans, and a relationship between MAO-B and neuro-degenerative diseases (such as Parkinson's disease) has been proposed.[3] The biological and medical importance of MAO, and the fact that it can convert simple substrates such as benzylamine, have encouraged researchers to a deep study of the reaction mechanism, both experimentally and theoretically (for an overview, see ref 4 and references therein). However, the mechanism is still under dispute.

The enzymatic reaction takes place in the "aromatic cage", a hydrophobic binding pocket inside the protein. The flavin adenine dinucleotide (FAD) coenzyme is part of this aromatic cage. It should be pointed out that, unlike in most other flavoenzymes, the flavin ring is covalently bonded to the protein via an 8α-thioether linkage; see Scheme 1. Two tyrosine residues are part of the aromatic cage (Tyr398 and Tyr435 in human MAO-B). It has been suggested[5] that they contribute to the reaction by polarizing the substrate amine lone pair.

MAO catalyzes the first step in the oxidative deamination of primary, secondary, and some tertiary amines. The amine is oxidized into its imine form while FAD is reduced to $FADH_2$.

Scheme 1. Chemical Structure of the Flavin Ring (a), and the Substrate (Benzylamine) In Its Protonated (b) and Unprotonated form (c)

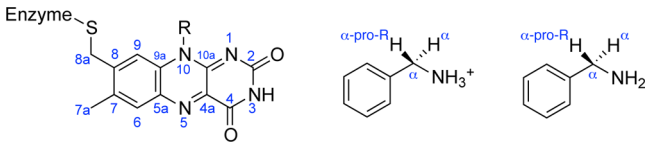

a) b) c)

In the next step, the imine is hydrolyzed nonenzymatically to the carbonyl. Consensus has been reached that the initial, and rate limiting, chemical step of the enzymatic reaction is the stereospecific[6,7] transfer of a hydrogen-α atom (pro-R) from the substrate to the FAD cofactor. Four possible types of mechanisms have been proposed (see Scheme 2): (a) a polar nucleophilic mechanism, in which the lone-pair of the amine group is transferred to FAD and the hydrogen moves as a proton (H^+);[8−10] (b) a radical mechanism in which the hydrogen is transferred as a neutral radical;[11,12] (c) the hydrogen is directly transferred as a hydride (H^-),[13] as in other flavoproteins;[14,15] or (d) a two step hydride transfer, where the first step is the hydride transfer and a flavin-substrate adduct formation, and the second step consists of an amine proton being transferred to N1 via two water molecules, while

Received: June 21, 2013
Revised: October 23, 2013
Published: October 28, 2013

   dx.doi.org/10.1021/jp4061522 | J. Phys. Chem. B 2013, 117, 14238−14246

Scheme 2. Proposed Reaction Mechanisms for MAO in the Literature[a]

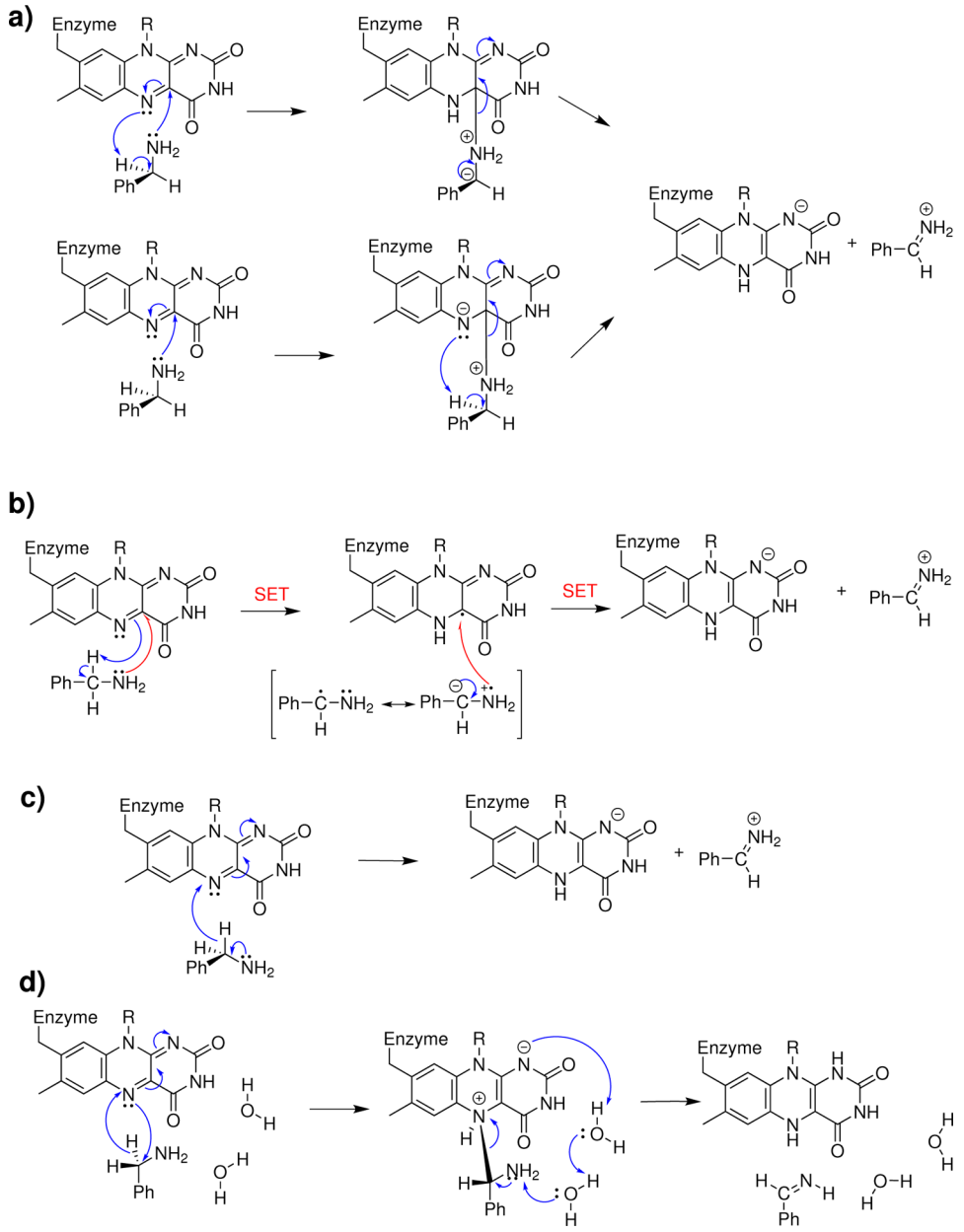

[a](a) Polar nucleophilic mechanism;[10] (b) radical mechanism;[12] (c) direct hydride transfer;[13−15] (d) two step hydride transfer.[16] SET refers to single electron transfer.

the adduct decomposes.[16] There are, however, experimental findings against the biradical mechanism (absence of electron paramagnetic resonance signal,[8,17] reduction potential[4]), supported by theoretical studies.[18] ^{15}N KIEs[10] studies are also against the hydride mechanism.

The crystal structures of human MAO-A and MAO-B have been resolved in the past decade with different accuracies ranging from 3.0[19,20] to 1.7 Å.[21] These ruled out a previously proposed[22,23] polar nucleophilic mechanism, in which a protein residue of the environment acts as a base for the proton abstraction.

Kinetic studies[8,24] on MAO-A and MAO-B show that there are strong kinetic isotope effects (KIEs) in the reaction rate. KIEs of k_H/k_D = 11.5 ± 0.6 (steady state) and k_H/k_D = 9.3 ± 1.2 (stopped flow kinetics for the rate limiting step) in MAO-A at 10.9 °C were found.,[8] while in MAO-B k_H/k_D = 4.7 ± 1.0 (steady state) at 25 °C.[24] Recently, ^{15}N KIE studies have indicated that the changes in the amine-N hybridization and H transfer are not concerted.[10]

The system has also been studied by computational techniques. H abstraction barriers for *p*-substituted benzylamines were calculated[9] using the semiempirical PM3 method, which supports the proposed polar nucleophilic mechanism. Evidence against biradical mechanisms was presented.[18] The functional role of the tyrosines within the aromatic cage was investigated at the Hartree−Fock/MM level.[25] Recently, gas-phase models[13,16] at the M06-2X level of theory (with some surrounding residues included at the semiempirical PM6 level[13]) lead to support of the hydride mechanism.

dx.doi.org/10.1021/jp4061522 | J. Phys. Chem. B 2013, 117, 14238−14246

MAO inhibitors also have been studied both experimentally[21,26] and theoretically[27−31] because of their potential use as pharmaceutical products.

However, to our knowledge, no QM/MM studies in which the whole protein has been taken into account have appeared so far. We have taken the active site geometries from molecular dynamics (MD) simulations instead of from crystal structure data to allow, for instance, the aromatic cage structure and water molecules within to adapt to the substrate under study. In this paper we focus on the reaction mechanism using state-of-the-art QM/MM calculations. These provide a clear answer on the course of the reaction mechanism.

CALCULATION DETAILS

The reaction mechanism has been calculated using a QM/MM approach. The crystal structure of human MAO-B with the inhibitor indole-2,3-dione (isatin)[21] determined at a resolution of 1.7 Å (PDB entry 1OJA) has been used as a starting geometry. We have replaced the isatin molecule by benzylamine and accordingly placed it closer to the flavin ring. Protonation states of protein residues were assigned based on the REDUCE code.[32] The full protein dimer was solvated in a pre-equilibrated box of TIP3P water[33] using VMD[34] version 1.9. We used the CHARMM27 force field.[35−41] Force field parameters for FAD and benzylamine have been constructed from homologous atoms already present in CHARMM27; partial charges were obtained from Löwdin population analysis in FIREBALL or natural population analysis in TURBOMOLE (see below) and slightly edited in order to mimic the trends of the homologous atoms in the CHARMM force field. These parameters only influence the initial MD run, not the following QM/MM calculations. Topology and parameter files can be found in the Supporting Information.

Two different MD runs have been carried out using NAMD,[42] one each for protonated and unprotonated benzylamine. The temperature has been set to 300 K by a Langevin thermostat, and a time step of 1 fs has been chosen. All bond lengths involving hydrogen atoms were frozen. For the equilibration process, cycles of minimization of 2000 steps followed by MD runs of 50 000 steps were performed, where the protein atoms were restrained (restrain parameters have been lowered each cycle: infinity (frozen protein atoms), 5.0, 2.0, and 0.1 kcal mol^{-1} $Å^{-2}$). This protocol allows water molecules to penetrate cavities within the protein. In the next step, a free MD of 3 ns was carried out; the Langevin piston Nosé-Hoover method was used to keep the system at 300 K and 1 bar. It should be noted that these MD simulations were only used to map the configuration space of the reactant structures. The temperature used is, therefore, not directly related to experimental conditions. Rates and KIEs have been calculated at different temperatures to match experimental conditions; see below.

Four snapshots have been taken for the unprotonated substrate, two for the protonated substrate. We chose the snapshots with the shortest C4a-N_{am}, C_α-N5, H_α-N5 distance, but sufficiently separated in time in order to have better statistics. In particular, we chose the snapshots at times 0.9688, 1.3822, 2.9212, 0.8500 ns (unprotonated substrates), and 1.8195, 2.6823 ns (protonated substrates). Of course, a sample of four snapshots cannot be expected to provide an accurate average of configurational space. However, as shown previously,[43] the entropic changes in the chemical step of an enzymatic reaction can often be neglected. These snapshots served as starting geometries for our QM/MM calculations, which have been carried out with the ChemShell suite.[44,45] ChemShell interfaces several QM and MM codes and takes care of the communication between the QM and MM parts. It also includes a robust and flexible geometry optimizer: DL-FIND.[46] The QM part comprised the whole substrate, the flavin ring (excluding C8a of the link to the protein, but including the methylene group between N10 and the rest of FAD), and some waters that may have some importance in the reaction; see Figures 1 and 4. In total, 48 (58) atoms were treated quantum

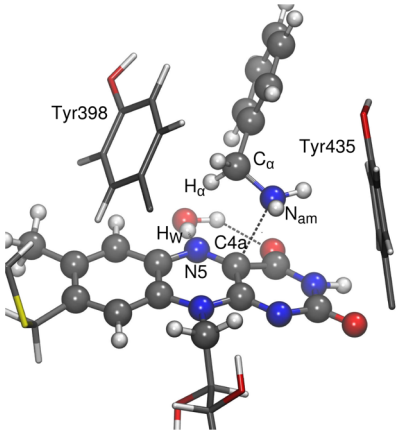

Figure 1. Reactant state of Snapshot 1. Atoms mentioned in the text are labeled. QM atoms are represented by ball and sticks. Residue Cys397 and the side chains of Tyr398 and Tyr435 are represented by sticks. Atom colors: white (H), gray (C), blue (N), red (O), yellow (S).

mechanically in the unprotonated (protonated) substrate calculations. Three more water molecules were included in the QM part when considering the protonated substrate for reasons given below. One chain of the protein dimer and all waters within 15 Å of the flavin ring and the substrate were included in the calculations as MM atoms: between 8422 and 8594 atoms, depending on the snapshot. We did not include the other protein chain (although it was included in the initial MD run) because its interaction with the catalytic center should be negligible (the chain is farther than 10 Å from the active site). All residues or water molecules with at least one atom within 8 Å of the flavin ring or the substrate were relaxed in the geometry optimizations.

Three different QM methods were used, all of them relying in density functional theory (DFT). The first one is the fireball method,[47−50] as implemented in FIREBALL.[49,51] We have used a simple optimized minimum basis[52] of numerical atomic orbitals (NAOs). The cutoff radii (NAOs are strictly zero beyond this cutoff radius[47]) are (in atomic units): 4.0 (*s*) for H, 4.0 (*s*) and 4.5 (*p*) for C, 3.6 (*s*) and 4.1 (*p*) for N and 3.3 (*s*) and 3.8 (*p*) for O. Exchange and correlation has been calculated using the Multicenter Weighted Exchange-correlation Density Approximation (McWEDA),[50] over the BLYP functional.[53,54] We have also employed the BP86 functional,[53,55] as implemented in TURBOMOLE version 6.03,[56] in combination with resolution of the identity and the def2-SVP basis set.[57] It has been shown by our group in a previous work[58] that enzymatic geometries obtained with BP86 and with B3LYP coincide very well. Single point calculations using the M06 functional,[59] as implemented in NWChem,[60] and a cc-pVTZ basis set[61] have also been carried out. Since natural (spin)

dx.doi.org/10.1021/jp4061522 | J. Phys. Chem. B 2013, 117, 14238−14246

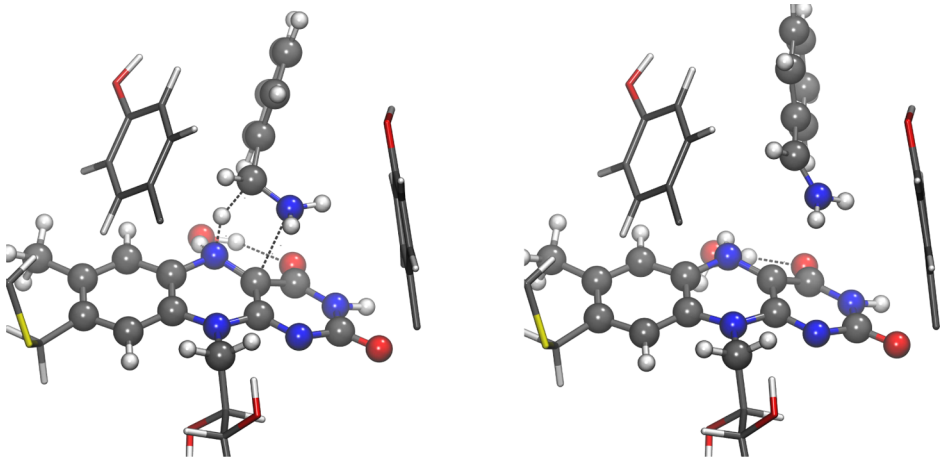

Figure 2. Geometries of the transition state (left) and product state (right) for Snapshot 1. See Figure 1 for the representation.

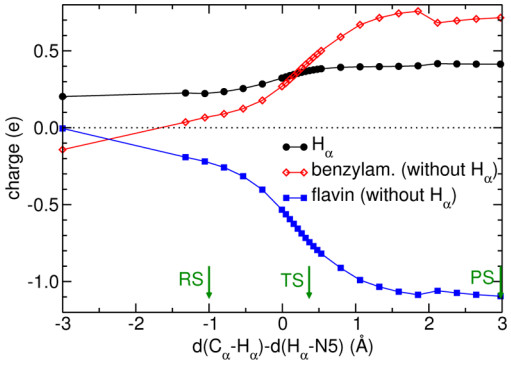

Figure 3. NBO charges of the reactive species during the course of the reaction for Snapshot 1. Note that H_α is included neither in the benzylamine nor in the flavin total charge, so values are different from the ones written in the text.

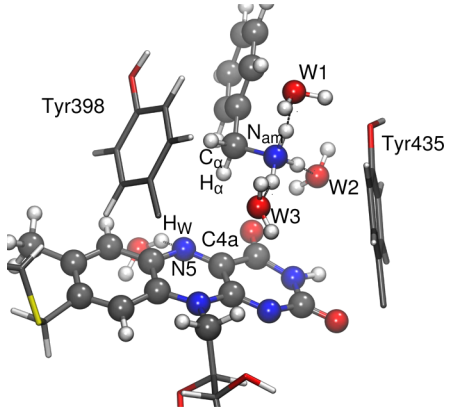

Figure 4. Reactant state of Snapshot 5. QM water molecules coordinated to the protonated amine group are shown. See Figure 1 for the representation.

population analysis can help us to distinguish between the four possible reaction mechanisms, we have performed it at the BP86 level. We have used the same CHARMM27 force field for the MM part as in the MD simulations, in DL_POLY.[62] With respect to the QM/MM interface, we have used an additive scheme, with electrostatic embedding. Hydrogen link atoms, with the charge shift scheme, were used for truncation of C−C bonds.

Geometries of the snapshots from the MD runs have been preoptimized using the fireball method for the QM part, and the DL-FIND optimizer,[46] followed by a more accurate optimization using BP86. Fireball preoptimization considerably reduces the number of optimization steps needed in BP86, thus improving the computational efficiency. This allows us to obtain an optimized geometry for the reactant state. After that, a potential energy surface scan has been carried out, using the distance difference $d(C_\alpha - H_\alpha) - d(H_\alpha - N5)$ as the reaction coordinate. The transition state has been found by means of the dimer method,[63] as implemented in DL-FIND,[64] using the geometries with the highest and second highest energies of the scan as the starting geometries.[64] Minimizations starting from all transitions states, which again ended up in reactant structures with negligible differences to the original ones, confimed smooth connections between reactant and transition states. In order to obtain accurate values for the energy barriers, single-point energy calculations at the optimized BP86 geometries with M06,[59] a quite reliable exchange-correlation functional for kinetics which also approximatively accounts for dispersion interactions, have been carried out. All energy values reported refer to M06 values. This combination of BP86 geometries and single point M06 calculations has been successfully used in our group for other studies.[65]

In order to obtain theoretical reaction rates and KIEs, two-point finite difference Hessian calculations of all QM atoms (except QM-water), as implemented in DL-FIND, have been carried out. The QM water was left out because its chemical environment is almost unchanged between the reactant and the transition states. Moreover, movement of the water with respect to FAD might lead to soft modes which reduce the numerical stability. A single imaginary frequency was obtained, even though the set of active atoms was smaller than in the optimizations. The transition modes consisted mainly of the movement of the hydrogen atom between substrate and cofactor. Thermal averages for the energy barriers have been calculated according to[66,67]

$$\Delta E^{\ddagger}_{\mathrm{av}} = -RT\ln\left(\frac{1}{n}\sum_{i=1}^{n}\exp\left(\frac{-\Delta E^{\ddagger}_{i}}{RT}\right)\right) \quad (1)$$

where n is the number of snapshots, $\Delta E^{\ddagger}_{i}$ are the energy barriers of the different snapshots, R is the ideal gas constant, and T = 298.2 K (25 °C) the temperature.

dx.doi.org/10.1021/jp4061522 | J. Phys. Chem. B 2013, 117, 14238−14246

KIEs have been calculated by taking into account the contribution of atom tunneling in an approximate manner. The crossover temperature T_c can be interpreted as the temperature below which tunneling significantly contributes to the reaction rate.[68]

$$T_c = \frac{\hbar\omega_b}{2\pi k_B} \quad (2)$$

where $\hbar$ is Planck's constant, k_B is Boltzmann's constant, and ω_b is the magnitude of the imaginary frequency of the unstable mode at the saddle point. Since T_c is well below room temperature (less than 150 K) in all cases studied and tunneling is comparatively weak, simple approximations for the tunneling contribution can be used. We used transition state theory with all vibrational degrees of freedom approximated by harmonic oscillators. Along the reaction coordinate, a symmetric Eckart barrier[69] was fitted to the reaction path in order to match the barrier height and ω_b. The quantum mechanical flux through that barrier, including all tunneling and nonclassical reflection contributions, can be calculated analytically. The rate was corrected by the ratio of the classical rate and the analytic rate via the Eckart barrier. Note that all degrees of freedom perpendicular to the transition mode are still treated as harmonic oscillators. The doubly deuterated α,α-[^{2}H]-benzylamine species has been used in KIEs calculations, in order to compare with experimental results.

RESULTS

As explained in the Introduction, four different mechanisms have been proposed in the literature. In all of these models, it is supposed that the benzylamine is in its unprotonated form, although the protonation state in reality is not known. At neutral pH the substrate is in the protonated state in solution, but due to the hydrophobic character of the aromatic cage,[21] it makes sense to assume that it loses its proton during transfer into the active site. There are also studies that consider that the catalysis works on the protonated form,[70] but they are controversial.[71,72] Recent theoretical pK_a calculations[72] do not clearly favor one substrate species over the other. Moreover, it was shown[72] that deprotonation in the aromatic cage is a relatively easy step, with a free energy deprotonation cost of only 8 kJ mol^{-1}. Since there is no clear evidence of the protonation state of the substrate, and it is very easy to change from one to the other, we have performed our calculations in both the unprotonated and the protonated form.

Experimental evidence and theoretical calculations claim against a biradical mechanism,[4,8,17,18] although there are some results in favor of this mechanism.[11,12] For the sake of completeness, we have also considered the feasibility of the biradical mechanism. This, together with geometrical changes during the reaction, will help us to decide which model is supported by our QM/MM calculations.

Unprotonated Benzylamine. In order to check the feasibility of the biradical mechanism, we have done open-shell calculations, for both triplet and open-shell singlet in the reactant and the transition state. Open-shell (unrestricted Kohn−Sham) singlet calculations lead to a symmetric distribution of the spin up and down densities in both the reactant state and the transition state, even when a highly asymmetric electron density is considered as an starting point. This means that the singlet state is actually a closed-shell singlet. The triplet state reactant has a BP86 energy 143 kJ mol^{-1} higher than the singlet state (in Snapshot 1), so the reaction will not proceed that way. Our results, thus, claim against the biradical reaction mechanism for the unprotonated substrate.

Reaction barriers were calculated in four different snapshots. The results are 91.0, 116.6, 231.7, and 97.7 kJ mol^{-1} for the four snapshots (they are reduced to 80.6, 107.4, 216.1, and 88.5 kJ mol^{-1} when we take into account zero-point (ZP) vibrational energies; see Table 1). The energy barriers of Snapshots 1 and 4 are small enough to proceed at room temperature. The thermally averaged energy barrier is 83.9 kJ mol^{-1}, which results in a rate constant of 0.55 min^{-1} at 25.0 °C. This is in reasonable agreement with the experimental rate constant of 600 ± 110 min^{-1} obtained for MAO-B,[24] considering the many idealizations in our theoretical treatment compared to experiment. The difference in the rate translates to a difference in the barrier of about 15 kJ mol^{-1}, which is roughly our expected accuracy. These results show that the unprotonated benzylamine is a feasible substrate for the H_α abstraction. Snapshots 1 and 4 are the ones with the lower energy barrier. The 25 kJ mol^{-1} difference between Snapshot 1 and Snapshot 2 is likely caused by the larger distance between benzylamine and the flavin ring in Snapshot 2. The energy barrier of Snapshot 3 is so high because benzylamine is placed in a way that there is no interaction between the N_{am} and C4a. Moreover, the pro-S H_α is closer to the flavin rather than the pro-R one. This agrees with the experimental finding that the enzyme is highly stereospecific:[6,7] a short N_{am}−C4a distance implies also that the pro-R H_α is closer to N5 than the pro-S one. The reaction energies ΔE_r are −4.9, +61.3, +88.9, and +42.4 kJ mol^{-1} for Snapshots 1−4, respectively. Snapshot 1, in contrast to the others, seems to be slightly exothermic. This low energy of the products, however, is caused by a water rearrangement happening after the transition state. When this is taken into account, the reaction is endothermic for Snapshot 1 as well. The rearranged waters do not play any role in the reaction. However, this shows the necessity to include several snapshots, in order to get rid of contributions from degrees of freedom not related to the reaction and, thus, to have a clear picture of the energetics of the reaction. It should be noted, however, that what is considered as a product here is in reality only an intermediate. An exothermic proton transfer to flavin, which forms $FADH_2$, follows the reaction studied here.

Table 1. Four Snapshots of Deprotonated Benzylamine

	Snapshot 1	Snapshot 2	Snapshot 3	Snapshot 4
$\Delta E^{\ddagger}$(kJ mol^{-1})	80.6	107.4	216.1	88.5
ΔE_r (kJ mol^{-1})	−4.9	+61.3	+88.9	+42.4
ω_b (cm^{-1})	466i	191i	183i	502i
T_c (K)	106.8	43.8	42.0	114.9
KIE @ 25 °C	3.5	2.4	2.7	3.7

KIEs were calculated for the doubly deuterated α,α-[^{2}H]benzylamine, in order to compare with experimental results. The H/D KIEs for the two snapshots with the low barriers (3.5 and 3.7) are in good agreement with the experimental data (4.7 ± 1.0 for MAO-B).[24] The $^{14}N/^{15}N$ KIE is 0.9841 in almost perfect agreement with the experimental[10] value of 0.9846 for the same enzyme (a correction for the equilibrium isotope effect on the deprotonation[10] was taken into account). For doubly deuterated substrate, the $^{14}N/^{15}N$ KIE increases, but it does

dx.doi.org/10.1021/jp4061522 | J. Phys. Chem. B 2013, 117, 14238−14246

so only very slightly (rounded as well to 0.9841), while the experimental value increases to 0.9901.

In Figure 1 we can see the reactant state of the first snapshot, the one with the lowest barrier. Here we are going to discuss only our results for this first snapshot; the geometries of other snapshots are qualitatively similar and can be found in the Supporting Information. In the reactant state, the H_α-N5 distance is 2.13 Å (Table 2); close enough for the flavin N5 to abstract H_α. N5 is in a slightly distorted sp^2 geometry, with a small portion of sp^3 hybridization, as can be seen from the angles in Table 2. In order to give a quantitative value to this sp^2–sp^3 mixing, we can use the partial hybridization index n, that can be obtained with the formula:[73]

$$1 + n\cos\theta = 0 \quad (3)$$

where θ is the average angle ∠R–N5–R. We obtain for N5 an $sp^{2.11}$ hybridization. The N_{am} in the amine group has a hybridization closer to sp^3 ($sp^{2.45}$), with the lone pair interacting with the C4a (carbon) as can be seen by the relatively small N_{am}–C4a distance (2.52 Å). This is clearly too large for a covalent bond, but also smaller than a normal nonbonded distance. The interaction between N_{am} and C4a is clearly attractive as it can be seen from the potential-energy scan along that distance given in the Supporting Information. Alternatively, the lone pair of N_{am} can form a hydrogen bond to a nearby water molecule, which is higher in energy than the association to the flavin-C4a, though.

Table 2. Selected Geometrical Parameters for the Reactant, Transition State, and Product of Snapshot 1

distances (Å)	reactant state	transition state	product state
$d(H_\alpha–N5)$	2.13	1.18	1.03
$d(H_\alpha–C_\alpha)$	1.12	1.55	4.01
$d(C_\alpha–N5)$	3.01	2.64	3.78
d(C4a–N5)	1.33	1.39	1.40
d(N5–C6a)	1.38	1.42	1.39
$d(N_{am}–C4a)$	2.52	2.56	2.97
$d(N_{am}–C_\alpha)$	1.45	1.36	1.32
$d(H_w–N5)$	1.78	1.86	2.80
angles (deg)	**reactant state**	**transition state**	**product state**
$\angle(C_\alpha–N_{am}–H1_{am})$	113.26	117.74	116.79
$\angle(C_\alpha–N_{am}–H2_{am})$	115.47	119.72	120.98
$\angle(H1_{am}–N_{am}–H2_{am})$	113.35	118.40	119.80
∠(C4a–N5–C6a)	118.22	114.92	119.37
$\angle(C4a–N5–H_\alpha)$	95.15	106.78	116.13
$\angle(C6a–N5–H_\alpha)$	107.86	111.20	115.77
$\angle(C_\alpha–H_\alpha–N5)$	132.99	150.07	69.85

There is a water molecule close to the N5 atom (see Figure 1 and Table 2). We tested whether N5 might preferably abstract the proton from the water molecule instead of abstracting H_α. We have seen that proton abstraction from water by N5 is a monotonously endothermic process, so this reaction cannot happen. Even if the proton is placed close to N5 using a restraint potential, it moves back to the water molecule as soon as this potential is removed.

In the transition state (see Figure 2), the H_α is already very close to the N5 atom (1.18 Å, Table 2). N_{am} has changed from an sp^3 to an sp^2 hybridization ($sp^{2.08}$), and the N_{am}–C_α distance has shortened from 1.45 Å to 1.36 Å, indicating a partial double bond character for N_{am}–C_α. This can be considered a confirmation that the amine has lost its lone pair. The C4a–N5 distance has increased slightly from 1.33 Å to 1.39 Å, implying that C4a–N5 bond has changed from a double bond to a single one. N5 is at an sp^3 geometry ($sp^{2.79}$) in the transition state. The distance from N_{am} to C4a has increased a bit from 2.52 Å to 2.56 Å.

In the product state, the N5 atom is almost planar ($sp^{2.18}$), its lone pair contributes to the π system of the flavin ring. N_{am}, on the other hand, is sp^2-hybridized ($sp^{2.05}$), like in the transition state. The amine lone pair is already transmitted to the flavin ring in the transition state.

During the reaction, a proton and an electron pair are transferred from the substrate to the flavin cofactor. In a hydride transfer, the electron pair would be transferred with the proton, in a polar nucleophilic mechanism, it would take the route via N_{am}-C4a. Apart from that, these two mechanisms are equivalent. Since electrons behave according to the laws of quantum mechanics, they are delocalized and can, in general, not be assigned to a specific atom. Thus, the real reaction is an intermediate case between the two extremes: a polar nucleophilic mechanism and a hydride transfer. However, in Snapshot 3, there is no N_{am}-C4a interaction for steric reasons. Thus, in this case the reaction has to proceed via a hydride transfer. Comparison between Snapshots 1 and 3, therefore, provides insight to the difference between the mechanisms.

We have performed a natural population analysis in order to elucidate the charges on the atoms in the reactant, transition, and product states; see Figure 3. In Snapshot 1, the total charges of benzylamine and flavin are +0.29 and −0.22, respectively, in the reactant state, while in the product state they are +0.72 and −0.68 (the total charge is not zero because of a slightly negatively charged QM water). In Snapshot 3, however, due to the pure hydride transfer, the total charges of benzylamine and flavin are +0.06 and +0.03, respectively, in the reactant state. The charges of the product state are with +0.66 and −0.62 for benzylamine and flavin (including H_α), similar to the ones of Snapshot 1. So, clearly, in the reactant of Snapshot 1, already about 30–40% of the charge is transferred from the substrate to the cofactor, while virtually no charge is transferred in the reactant state of Snapshot 3. Charge transfer only starts close to the transition state in Snapshot 3. This suggests a mostly polar nucleophilic mechanism, in good agreement with previous theoretical[9] and experimental[8] proposals, but at variance with recent gas-phase DFT calculations.[13,16] The pure hydride transfer from Snapshot 3 has a significantly higher barrier.

These changes in the charges in Snapshot 1 can be explained by an electron pair being transferred from the substrate to the flavin cofactor concurrently with the proton transfer. It is likely that the amine lone pair is transferred. Our analysis demonstrates that proton and electrons are transferred in a concerted but asynchronous way: the electron pair is transferred at least mostly via the N_{am}-C4a interaction rather than together with the proton by a hydride transfer.

We investigated a possible functional role of the residues Tyr398, Tyr435 (see Figure 1). It is suggested that they polarize the substrate amine lone pair, favoring the N_{am}-C4a interaction, and thereby diminishing the energy barrier.[5] We have checked the effect of these residues on the barrier height. To do so, we have removed all charges from the side chain, thus taking away possible dipole–dipole interactions between the tyrosines and the substrate. Our results show that tyrosine charges do not affect the barrier height too much (the energy difference is less than 1 kJ mol^{-1}). This is consistent with

dx.doi.org/10.1021/jp4061522 | J. Phys. Chem. B 2013, 117, 14238–14246

experiments,[5] showing that the rate constants k_{cat} of the wild type and a Y435F mutant (i.e., tyrosine substituted by phenylalanine, which has no dipole moment) are very similar. Addition of the side chains of both tyrosines to the QM part does not alter our reaction barriers too much either (less than 3 kJ mol^{-1}, less than 6 kJ mol^{-1} if the dispersion-corrected[74] functional BP86-D is used). The three phenyl rings are not aligned, and spatially too distant to directly interact by π-stacking (see Supporting Information). We conclude, thus, that a functional role of Tyr398 and Tyr435 is not related to decreasing the energy barrier. The residues may, of course, help for the substrate to be placed in a position that enhances attack by the flavin ring. However, this is outside the scope of this work.

Protonated Benzylamine. As in the unprotonated case, we have first performed open-shell calculations to test a biradical mechanism for the protonated form of the substrate. The reactant state is a closed-shell singlet, but the transition state is a singlet biradical. The triplet state energy is 152.4 kJ mol^{-1} higher than the singlet in the reactant state (for Snapshot 5). So the reaction will not proceed through the triplet channel.

There is significant spin density of different sign in benzylamine and the flavin ring. Thus, for the protonated benzylamine, the reaction proceeds via a radical mechanism. In particular, the spin density in benzylamine is strongly located at the C_α, while in flavin it is essentially delocalized over the ring (see Supporting Information for details).

The energy barriers are, with 253.0 and 278.1 kJ mol^{-1} (239.0 and 263.2 kJ mol^{-1} if we take into account the ZP vibrational energies) for the two snapshots, significantly too high for the reaction to proceed at room temperature. Thus, a detailed discussion will not help to understand the reaction mechanism. However, details are provided in the Supporting Information.

Table 3. Two Snapshots of Protonated Benzylamine

	Snapshot 5	Snapshot 6
$\Delta E^{\ddagger}$ (kJmol^{-1})	239.0	263.2
ΔE_r (kJmol^{-1})	+128.7	+245.5
ω_b (cm^{-1})	416i	501i
T_c (K)	95.2	114.8
KIE @ 25 °C	2.8	3.9

It is interesting to point out here that the water molecules, which form H bonds with the benzylamine protons, are not able to abstract these. We have found that none of the three waters can abstract a proton from the amine group. If the proton is placed on the water molecule with restraint potentials, it moves back to the amine as soon as the restraint is removed. This tells us that unprotonated benzylamine plus an hydronium ion is not a stable configuration. The question of how the benzylamine loses a proton on its way into the binding pocket is outside the scope of this work.

A different mechanism had been proposed for protonated benzylamine based on gas phase calculations.[16] The conclusion, however, is the same as ours, that the reaction cannot proceed this way because of the large energy barrier (180 kJ mol^{-1}).

DISCUSSION AND CONCLUSION

In this paper we report on QM/MM calculations for the reaction mechanism of MAO. To the best of our knowledge, this is the first time that full QM/MM calculations on that system have been done. We have also calculated the KIEs of this reaction for the first time. We used the Eckart approximation, which is justified by the small crossover temperature for tunneling in this reaction (less than 150 K).

The resulting mechanism is not a textbook polar nucleophilic mechanism; the reaction has also some hydride-transfer character. In fact, a polar nucleophilic mechanism and a hydride transfer can only be distinguished by the path the electrons take. Their quantum nature, however, makes a clear distinction impossible. Overall, it is similar to the one proposed by Miller and Edmondson,[8] and supported by theoretical investigations.[9,25] While they propose an intermediate adduct, our results support concerted reaction in one step. The proton and lone pair transfers to the flavin ring occur in a concerted (but asynchronous) way. This means that, in the transition state, the amine lone pair is already almost completely transmitted to the flavin ring, as can be seen by the nearly sp^2 structure in the transition state. This is in agreement with experimental results by MacMillar et al.[10] that the nitrogen bond change should precede or succeed the rate-limiting proton transfer. Our mechanism is depicted in Scheme 3.

Hydrogen abstraction from protonated benzylamine has a very high barrier. Thus, the reaction proceeds via unprotonated substrate.

Hydrogen abstraction from the unprotonated form has a thermally averaged energy barrier of 83.9 kJ mol^{-1} (at 25 °C). The spin state of the unprotonated system is found to be a real singlet at all stages of the reaction, which rules out the H atom transfer mechanism. Natural population analysis shows that about one-third of the charge is already transferred from the substrate to flavin in the reactant state complex. This is an indication of a polar nucleophilic contribution. The pure hydride transfer observed in Snapshot 3 does not show such a charge transfer in the reactant state. Its barrier is about 150 kJ mol^{-1} higher than the ones observed in the other snapshots.

ASSOCIATED CONTENT

Supporting Information

Images of the geometries of Snapshots 2−6, as well as tables with selected geometrical parameters, potential energy surface scan along the N_{am}−C4a distance, NBO analysis of Snapshot 3,

Scheme 3. Our Proposed Mechanism

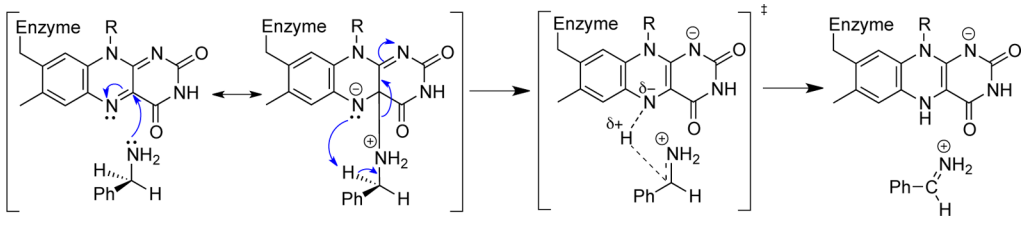

dx.doi.org/10.1021/jp4061522 | J. Phys. Chem. B 2013, 117, 14238−14246

as well as discussion of the reaction mechanism of protonated benzylamine. This material is available free of charge via the Internet at http://pubs.acs.org.

AUTHOR INFORMATION

Corresponding Author

*E-mail: kaestner@theochem.uni-stuttgart.de. Phone: +49 711 685 64473. Fax: +49 711 685 64442.

Notes

The authors declare no competing financial interest.

ACKNOWLEDGMENTS

This work was financially supported by the Alexander von Humboldt foundation as well as by the Baden-Württemberg Stiftung. The authors gratefully acknowledge Jesús I. Mendieta-Moreno and co-workers for their work on the fireball basis set used in this paper, as well as for their help in technical details.

REFERENCES

(1) Bach, A. W.; Lan, N. C.; Johnson, D. L.; Abell, C. W.; Bembenek, M. E.; Kwan, S. W.; Seeburg, P. H.; Shih, J. C. cDNA Cloning Of Human Liver Monoamine Oxidase A And B: Molecular Basis Of Differences In Enzymatic Properties. *Proc. Natl. Acad. Sci. U.S.A.* **1988**, *85*, 4934−8.

(2) Quitkin, F.; Rifkin, A.; Klein, D. F. Monoamine Oxidase Inhibitors. A Review of Antidepressant Effectiveness. *Arch. Gen. Psychiat.* **1979**, *36*, 749−760.

(3) Kumar, M. J.; Nicholls, D. G.; Andersen, J. K. Oxidative α-Ketoglutarate Dehydrogenase Inhibition Via Subtle Elevations In Monoamine Oxidase B Levels Results In Loss Of Spare Respiratory Capacity: Implications For Parkinson's Disease. *J. Biol. Chem.* **2003**, *278*, 46432−9.

(4) Edmondson, D. E.; Binda, C.; Mattevi, A. Structural Insights Into The Mechanism Of Amine Oxidation By Monoamine Oxidases A And B. *Arch. Biochem. Biophys.* **2007**, *464*, 269−76.

(5) Li, M.; Binda, C.; Mattevi, A.; Edmondson, D. E. Functional Role Of The "Aromatic Cage" In Human Monoamine Oxidase B: Structures And Catalytic Properties Of Tyr435 Mutant Proteins. *Biochemistry* **2006**, *45*, 4775−84.

(6) Belleau, B.; Fang, M.; Burba, J.; Moran, J. The Absolute Optical Specificity Of Monoamine Oxidase. *J. Am. Chem. Soc.* **1960**, *82*, 5752−5754.

(7) Yu, P. H.; Bailey, B. A.; Durden, D. A.; Boulton, A. A. Stereospecific Deuterium Substitution At The α-Carbon Position Of Dopamine And Its Effect On Oxidative Deamination Catalyzed By MAO-A And MAO-B From Different Tissues. *Biochem. Pharmacol.* **1986**, *35*, 1027−1036.

(8) Miller, J. R.; Edmondson, D. E. Structure-Activity Relationships In The Oxidation Of Para-Substituted Benzylamine Analogues By Recombinant Human Liver Monoamine Oxidase A. *Biochemistry* **1999**, *38*, 13670−83.

(9) Erdem, S. S.; Karahan, O.; Yildiz, I.; Yelekçi, K. A Computational Study On The Amine-Oxidation Mechanism Of Monoamine Oxidase: Insight Into The Polar Nucleophilic Mechanism. *Org. Biomol. Chem.* **2006**, *4*, 646−58.

(10) MacMillar, S.; Edmondson, D. E.; Matsson, O. Nitrogen Kinetic Isotope Effects For The Monoamine Oxidase B-Catalyzed Oxidation Of Benzylamine And (1,1-$^2H_2$)Benzylamine: Nitrogen Rehybridization And CH Bond Cleavage Are Not Concerted. *J. Am. Chem. Soc.* **2011**, *133*, 12319−21.

(11) Silverman, R. B. Radical Ideas about Monoamine Oxidase. *Acc. Chem. Res.* **1995**, *28*, 335−342.

(12) Lu, X.; Ji. H.; Silverman, R. B. In *Flavins and Flavoproteins*; Chapman, S., Perham, R., Scrutton, N., Eds.; Rudolf Weber Agency for Scientific Publications: Berlin, 2002; pp 817−830.

(13) Akyüz, M. A.; Erdem, S. S. Computational Modeling Of The Direct Hydride Transfer Mechanism For The MAO Catalyzed Oxidation Of Phenethylamine And Benzylamine: ONIOM (QM/QM) Calculations. *J. Neural Transm.* **2013**, *120*, 937−945.

(14) Kurtz, K. A.; Rishavy, M. A.; Cleland, W. W.; Fitzpatrick, P. F. Nitrogen Isotope Effects As Probes of the Mechanism of D-Amino Acid Oxidase. *J. Am. Chem. Soc.* **2000**, *122*, 12896−12897.

(15) Fitzpatrick, P. F. Oxidation of Amines by Flavoproteins. *Arch. Biochem. Biophys.* **2010**, *493*, 13−25.

(16) Vianello, R.; Repič, M.; Mavri, J. How are Biogenic Amines Metabolized by Monoamine Oxidases? *Eur. J. Org. Chem.* **2012**, *2012*, 7057−7065.

(17) Ramsay, R. R.; Upadhyay, A. K.; Li, M.; Edmondson, D. E. In *Flavins and Flavoproteins*; Nishino, T., Miura, R., Fukui, K., Tanokura, M., Eds.; ArchiTect, Inc, 2005; pp 137−142.

(18) Erdem, S. S.; Büyükmenekse, B. Computational Investigation On The Structure-Activity Relationship Of The Biradical Mechanism For Monoamine Oxidase. *J. Neural Transm.* **2011**, *118*, 1021−9.

(19) De Colibus, L.; Li, M.; Binda, C.; Lustig, A.; Edmondson, D. E.; Mattevi, A. Three-Dimensional Structure Of Human Monoamine Oxidase A (MAO A): Relation To The Structures Of Rat MAO A and Human MAO B. *Proc. Natl. Acad. Sci. U.S.A.* **2005**, *102*, 12684−9.

(20) Binda, C.; Newton-Vinson, P.; Hubálek, F.; Edmondson, D. E.; Mattevi, A. Structure Of Human Monoamine Oxidase B, A Drug Target For The Treatment Of Neurological Disorders. *Nat. Struct. Biol.* **2002**, *9*, 22−6.

(21) Binda, C.; Li, M.; Hubalek, F.; Restelli, N.; Edmondson, D. E.; Mattevi, A. Insights Into The Mode Of Inhibition Of Human Mitochondrial Monoamine Oxidase B From High-Resolution Crystal Structures. *Proc. Natl. Acad. Sci. U.S.A.* **2003**, *100*, 9750−5.

(22) Hamilton, G. A.; Brown, L. E. Model Reactions And A General Mechanism For Flavoenzyme-Catalyzed Dehydrogenations. *J. Am. Chem. Soc.* **1970**, *92*, 7225−7227.

(23) Kim, J. M.; Bogdan, M. A.; Mariano, P. S. Mechanistic Analysis Of The 3-Methyllumiflavin-Promoted Oxidative Deamination Of Benzylamine. A Potential Model For Monoamine Oxidase Catalysis. *J. Am. Chem. Soc.* **1993**, *115*, 10591−10595.

(24) Newton-Vinson, P.; Hubalek, F.; Edmondson, D. E. The Aromatic Cage In The Active Site Of Monoamine Oxidase B: Effect On The Structural And Electronic Properties Of Bound Benzylamine And *p*-Nitrobenzylamine. *Protein Express. Purif.* **2000**, *20*, 334−45.

(25) Akyüz, M. A.; Erdem, S. S.; Edmondson, D. E. The Aromatic Cage In The Active Site Of Monoamine Oxidase B: Effect On The Structural And Electronic Properties Of Bound Benzylamine And p-Nitrobenzylamine. *J. Neural Transm.* **2007**, *114*, 693−8.

(26) Zeller, E.; Barsky, J. In Vivo Inhibition Of Liver And Brain Monoamine Oxidase By 1-Isonicotinyl-2-Isopropyl Hydrazine. *Proc. Soc. Exp. Biol. Med.* **1952**, 459.

(27) Ferino, G.; Vilar, S.; Matos, J.; Uriarte, M.; Cadoni, E.; Monoamine Oxidase, E. Inhibitors: Ten Years of Docking Studies. *Curr. Top. Med. Chem.* **2012**, *12*, 2145−2162.

(28) Borštnar, R.; Repič, M.; Kržan, M.; Mavri, J.; Vianello, R. Irreversible Inhibition of Monoamine Oxidase B by the Antiparkinsonian Medicines Rasagiline and Selegiline: A Computational Study. *Eur. J. Org. Chem.* **2011**, *2011*, 6419−6433.

(29) Pavlin, M.; Mavri, J.; Repič, M.; Vianello, R. Quantum-Chemical Approach To Determining The High Potency Of Clorgyline As An Irreversible Acetylenic Monoamine Oxidase Inhibitor. *J. Neural Transm.* **2013**, *120*, 875−882.

(30) Erdem, S. S.; Türkkan, S.; Yelekçi, K.; Gökhan-Kelekçi, N. Insights Into The Binding Mode Of New N-Substituted Pyrazoline Derivatives To MAO-A: Docking And Quantum Chemical Calculations. *J. Neural Transm.* **2013**, *120*, 859−862.

(31) Erdem, S. S.; Özpnar, G. A.; Boz, U. Quantum Chemical Modeling Of The Inhibition Mechanism Of Monoamine Oxidase By Oxazolidinone And Analogous Heterocyclic Compounds. *J. Enzyme Inhib. Med. Chem.* **2013**, DOI: 10.3109/14756366.2012.753882.

(32) Word, J. M.; Lovell, S. C.; Richardson, J. S.; Richardson, D. C. Asparagine And Glutamine: Using Hydrogen Atom Contacts In The Choice Of Side-Chain Amide Orientation. *J. Mol. Biol.* **1999**, *285*, 1735−47.

(33) Jorgensen, W. L.; Chandrasekhar, J.; Madura, J. D.; Impey, R. W.; Klein, M. L. Comparison Of Simple Potential Functions For Simulating Liquid Water. *J. Chem. Phys.* **1983**, *79*, 926.
(34) Humphrey, W.; Dalke, A.; Schulten, K. VMD: Visual Molecular Dynamics. *J. Mol. Graphics* **1996**, *14* (33−8), 27−8.
(35) Mackerell, A. D.; Feig, M.; Brooks, C. L. Extending The Treatment Of Backbone Energetics In Protein Force Fields: Limitations Of Gas-Phase Quantum Mechanics In Reproducing Protein Conformational Distributions In Molecular Dynamics Simulations. *J. Comput. Chem.* **2004**, *25*, 1400−15.
(36) MacKerell, A. D., Jr.; Bashford, D.; Bellott, M.; Dunbrack, R. L., Jr.; Evanseck, J. D.; Field, M. J.; Fischer, S.; Gao, J.; Guo, H.; Ha, S.; et al. All-Atom Empirical Potential for Molecular Modeling and Dynamics Studies of Proteins. *J. Phys. Chem. B* **1998**, *102*, 3586−3616.
(37) Feller, S. E.; Gawrisch, K.; MacKerell, A. D., Jr. Polyunsaturated Fatty Acids In Lipid Bilayers: Intrinsic And Environmental Contributions To Their Unique Physical Properties. *J. Am. Chem. Soc.* **2002**, *124*, 318−26.
(38) Feller, S. E.; MacKerell, A. D., Jr. An Improved Empirical Potential Energy Function for Molecular Simulations of Phospholipids. *J. Phys. Chem. B* **2000**, *104*, 7510−7515.
(39) Schlenkrich, M.; Brickmann, J.; MacKerell,, A. D., Jr.; Karplus, M. In *Biological Membranes: A Molecular Perspective from Computation and Experiment*; Merz, K. M., Roux, B., Eds.; Birkhauser Boston Inc: Boston, 1996; pp 31−81.
(40) Foloppe, N.; MacKerell, A. D., Jr. All-Atom Empirical Force Field For Nucleic Acids: I. Parameter Optimization Based On Small Molecule And Condensed Phase Macromolecular Target Data. *J. Comput. Chem.* **2000**, *21*, 86−104.
(41) MacKerell, A. D.; Banavali, N. K. All-Atom Empirical Force Field For Nucleic Acids: II. Application To Molecular Dynamics Simulations Of DNA And RNA In Solution. *J. Comput. Chem.* **2000**, *21*, 105−120.
(42) Phillips, J. C.; Braun, R.; Wang, W.; Gumbart, J.; Tajkhorshid, E.; Villa, E.; Chipot, C.; Skeel, R. D.; Kalé, L.; Schulten, K. Scalable Molecular Dynamics with NAMD. *J. Comput. Chem.* **2005**, *26*, 1781−802.
(43) Senn, H. M.; Kästner, J.; Breidung, J.; Thiel, W. Finite-temperature effects in enzymatic reactions − Insights from QM/MM free-energy simulations. *Can. J. Chem.* **2009**, *87*, 1322−1337.
(44) ChemShell, a Computational Chemistry Shell; see www.chemshell.org.
(45) Metz, S.; Kästner, J.; Sokol, A. A.; Keal, T. W.; Sherwood, P. ChemShell−A Modular Software Package for QM/MM Simulations. *Comput. Mol. Sci.* **2013**, DOI: 10.1002/wcms.1163.
(46) Kästner, J.; Carr, J. M.; Keal, T. W.; Thiel, W.; Wander, A.; Sherwood, P. DL-FIND: An Open-Source Geometry Optimizer For Atomistic Simulations. *J. Phys. Chem. A* **2009**, *113*, 11856−65.
(47) Sankey, O.; Niklewski, D. Ab Initio Multicenter Tight-Binding Model For Molecular-Dynamics Simulations And Other Applications In Covalent Systems. *Phys. Rev. B* **1989**, *40*, 3979−3995.
(48) Demkov, A.; Ortega, J.; Sankey, O.; Grumbach, M. Electronic Structure Approach For Complex Silicas. *Phys. Rev. B* **1995**, *52*, 1618−1630.
(49) Lewis, J.; Glaesemann, K.; Voth, G.; Fritsch, J.; Demkov, A.; Ortega, J.; Sankey, O. Further Developments In The Local-Orbital Density-Functional-Theory Tight-Binding Method. *Phys. Rev. B* **2001**, *64*, 195103.
(50) Jelínek, P.; Wang, H.; Lewis, J.; Sankey, O.; Ortega, J. Multicenter Approach To The Exchange-Correlation Interactions In Ab Initio Tight-Binding Methods. *Phys. Rev. B* **2005**, *71*, 235101.
(51) Lewis, J. P.; Jelínek, P.; Ortega, J.; Demkov, A. A.; Trabada, D. G.; Haycock, B.; Wang, H.; Adams, G.; Tomfohr, J. K.; Abad, E.; et al. Advances And Applications In The FIREBALL Ab Initio Tight-Binding Molecular-Dynamics Formalism. *Phys. Status Solidi B* **2011**, *248*, 1989−2007.
(52) Basanta, M. A.; Dappe, Y. J.; Jelínek, P.; Ortega, J. Optimized Atomic-Like Orbitals For First-Principles Tight-Binding Molecular Dynamics. *Comput. Mater. Sci.* **2007**, *39*, 759−766.
(53) Becke, A. D. Density-Functional Exchange-Energy Approximation With Correct Asymptotic Behavior. *Phys. Rev. A* **1988**, *38*, 3098−3100.
(54) Lee, C.; Yang, W.; Parr, R. G. Development Of The Colle-Salvetti Correlation-Energy Formula Into A Functional Of The Electron Density. *Phys. Rev. B* **1988**, *37*, 785−789.
(55) Perdew, J. Density-Functional Approximation For The Correlation Energy Of The Inhomogeneous Electron Gas. *Phys. Rev. B* **1986**, *33*, 8822−8824.
(56) TURBOMOLE v 6.0.3 2009, a development of University of Karlsruhe and Forschungszentrum Karlsruhe GmbH, 1989−2007, TURBOMOLE GmbH, since 2007; available from http://www.turbomole.com.
(57) Schäfer, A.; Horn, H.; Ahlrichs, R. Fully Optimized Contracted Gaussian Basis Sets For Atoms Li to Kr. *J. Chem. Phys.* **1992**, *97*, 2571.
(58) Rommel, J. B.; Kästner, J. The Fragmentation-Recombination Mechanism Of The Enzyme Glutamate Mutase Studied By QM/MM Simulations. *J. Am. Chem. Soc.* **2011**, *133*, 10195−203.
(59) Zhao, Y.; Truhlar, D. G. A New Local Density Functional For Main-Group Thermochemistry, Transition Metal Bonding, Thermochemical Kinetics, And Noncovalent Interactions. *J. Chem. Phys.* **2006**, *125*, 194101.
(60) Valiev, M.; Bylaska, E. J.; Govind, N.; Kowalski, K.; Straatsma, T. P.; Van Dam, H. J. J.; Wang, D.; Nieplocha, J.; Apra, E.; Windus, T. L.; et al. NWChem: A Comprehensive And Scalable Open-Source Solution For Large Scale Molecular Simulations. *Comput. Phys. Commun.* **2010**, *181*, 1477−1489.
(61) Dunning, T. H. Gaussian Basis Sets For Use In Correlated Molecular Calculations. I. The Atoms Boron Through Neon And Hydrogen. *J. Chem. Phys.* **1989**, *90*, 1007.
(62) Smith, W.; Yong, C.; Rodger, P. DL_POLY: Application To Molecular Simulation. *Mol. Simul.* **2002**, *28*, 385−471.
(63) Henkelman, G.; Jonsson, H. A Dimer Method For Finding Saddle Points On High Dimensional Potential Surfaces Using Only First Derivatives. *J. Chem. Phys.* **1999**, *111*, 7010.
(64) Kästner, J.; Sherwood, P. Superlinearly Converging Dimer Method For Transition State Search. *J. Chem. Phys.* **2008**, *128*, 014106.
(65) Rommel, J. B.; Liu, Y.; Werner, H.-J.; Kästner, J. Role Of Tunneling In The Enzyme Glutamate Mutase. *J. Phys. Chem. B* **2012**, *116*, 13682−9.
(66) Lonsdale, R.; Harvey, J. N.; Mulholland, A. J. Compound I Reactivity Defines Alkene Oxidation Selectivity in Cytochrome P450cam. *J. Phys. Chem. B* **2010**, *114*, 1156−1162.
(67) Kästner, J.; Sherwood, P. The Ribosome Catalyses Peptide Bond Formation By Providing High Ionic Strength. *Mol. Phys.* **2010**, *108*, 293.
(68) Gillan, M. J. Quantum-Classical Crossover Of The Transition Rate In The Damped Double Well. *J. Phys. C* **1987**, *20*, 3621.
(69) Eckart, C. The Penetration of a Potential Barrier by Electrons. *Phys. Rev.* **1930**, *35*, 1303.
(70) Jones, T. Z. E.; Balsa, D.; Unzeta, M.; Ramsay, R. R. Variations In Activity And Inhibition With pH: The Protonated Amine Is The Substrate For Monoamine Oxidase, But Uncharged Inhibitors Bind Better. *J. Neural Transm.* **2007**, *114*, 707−12.
(71) Dunn, R. V.; Marshall, K. R.; Munro, A. W.; Scrutton, N. S. The pH Dependence Of Kinetic Isotope Effects In Monoamine Oxidase A Indicates Stabilization Of The Neutral Amine In The Enzyme-Substrate Complex. *FEBS J.* **2008**, *275*, 3850−8.
(72) Borštnar, R.; Repič, M.; Kamerlin, S. C. L.; Vianello, R.; Mavri, J. Computational Study of the pK_a Values of Potential Catalytic Residues in the Active Site of Monoamine Oxidase B. *J. Chem. Theory Comput.* **2012**, *8*, 3864−3870.
(73) Anslyn, E. V.; Dougherty, D. A. *Modern Physical Organic Chemistry*; University Science Books, 2006; p 10.
(74) Grimme, S. Semiempirical GGA-Type Density Functional Constructed With A Long-Range Dispersion Contribution. *J. Comput. Chem.* **2006**, *27*, 1787−1799.